

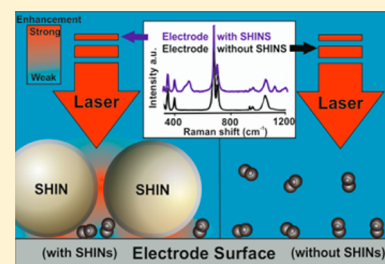
Utilizing in Situ Electrochemical SHINERS for Oxygen Reduction Reaction Studies in Aprotic Electrolytes

Thomas A. Galloway and Laurence J. Hardwick*

Stephenson Institute for Renewable Energy, Department of Chemistry, University of Liverpool, Liverpool L69 7ZD, United Kingdom

S Supporting Information

ABSTRACT: Spectroscopic detection of reaction intermediates upon a variety of electrode surfaces is of major interest within physical chemistry. A notable technique in the study of the electrochemical interface has been surface-enhanced Raman spectroscopy (SERS). The drawback of SERS is that it is limited to roughened gold and silver substrates. Herein we report that shell-isolated nanoparticles for enhanced Raman spectroscopy (SHINERS) can overcome the limitations of SERS and has followed the oxygen reduction reaction (ORR), within a nonaqueous electrolyte, on glassy carbon, gold, palladium, and platinum disk electrodes. The work presented demonstrates SHINERS for spectroelectrochemical studies for applied and fundamental electrochemistry in aprotic electrolytes, especially for the understanding and development of future metal–oxygen battery applications. In particular, we highlight that with the addition of Li^+ , both the electrode surface and solvent influence the ORR mechanism, which opens up the possibility of tailoring surfaces to produce desired reaction pathways.



Understanding the electrochemistry of oxygen in non-aqueous electrolyte media is of great interest, in particular, for the development of metal-air batteries,^{1,2} where the formulation of a stable electrolyte is a major challenge and so far has inhibited their development.^{3–5} The oxygen reduction and oxidation reaction mechanisms can be complex, involving multiple intermediates, and are highly dependent upon the solvent used.^{5–7} There have been a number of recent studies on the development of the electrolyte media,^{8,9} using a variety of analytical and spectroscopic techniques.^{9–12} In particular, surface-enhanced Raman spectroscopy (SERS)¹³ has been shown to be a valuable technique; however, it is limited by the surfaces that it can be used to analyze, essentially gold and silver.^{14,15}

The Raman effect is very weak (1 photon in ca. 10 million is inelastically scattered).¹⁶ The signal can be enhanced up to ca. 10^{11} by roughening the electrode surface, using an electrochemical oxidation/reduction cycle (ORC).¹⁷ SERS is a nondestructive and noninvasive technique; it can be used to investigate the chemical bonding of surface species, making it a valuable technique to study in situ the oxygen reduction and evolution reactions (ORR and OER), taking place at the electrode interface.¹⁸ SERS has been used to study the ORR and OER reaction on Au in metal–oxygen batteries¹⁹ and has shown the effect of varying the alkyl chain length in the supporting salt.²⁰ SERS studies with respect to ORR have so far been limited in the main to Au surfaces, but there is significant interest to study these reactions on non-SERS surfaces, such as carbon, a prominent option as a future cathode material.²¹ Unlike SERS the use of SHINERS (shell isolated nanoparticles for enhanced Raman spectroscopy) is not restricted to precious metal surfaces. Adding a near-monolayer of SHINs can enhance the Raman signal by ca. 10^8 .²² SHINs consist of a gold core,

surrounded by a very thin (2 to 3 nm) uniform SiO_2 shell (Figure 1). The shell thickness is very important; a shell greater

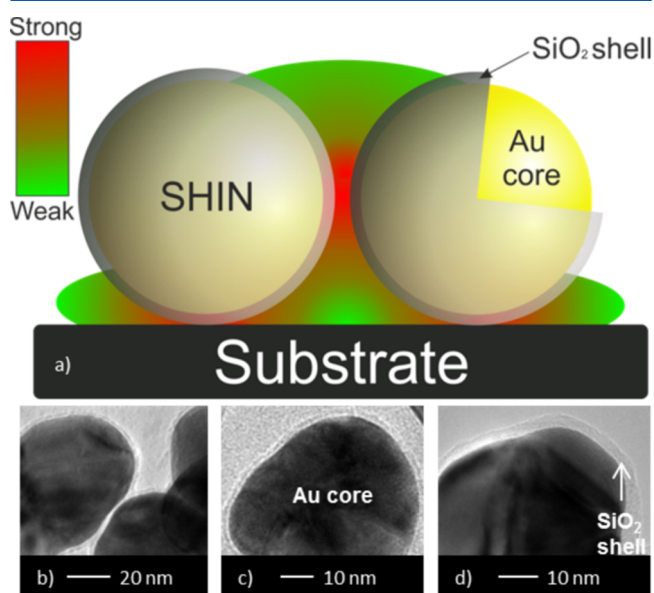


Figure 1. (a) Schematic diagram of SHINs on a substrate showing the electromagnetic field distribution between SHINs (see the graduated color key where red = strong and green = weak enhancement). TEM images (b,c) of SHINs at different resolutions with a 2 nm shell and (d) example of a 3.5 nm shell particle.

Received: April 1, 2016

Accepted: May 19, 2016

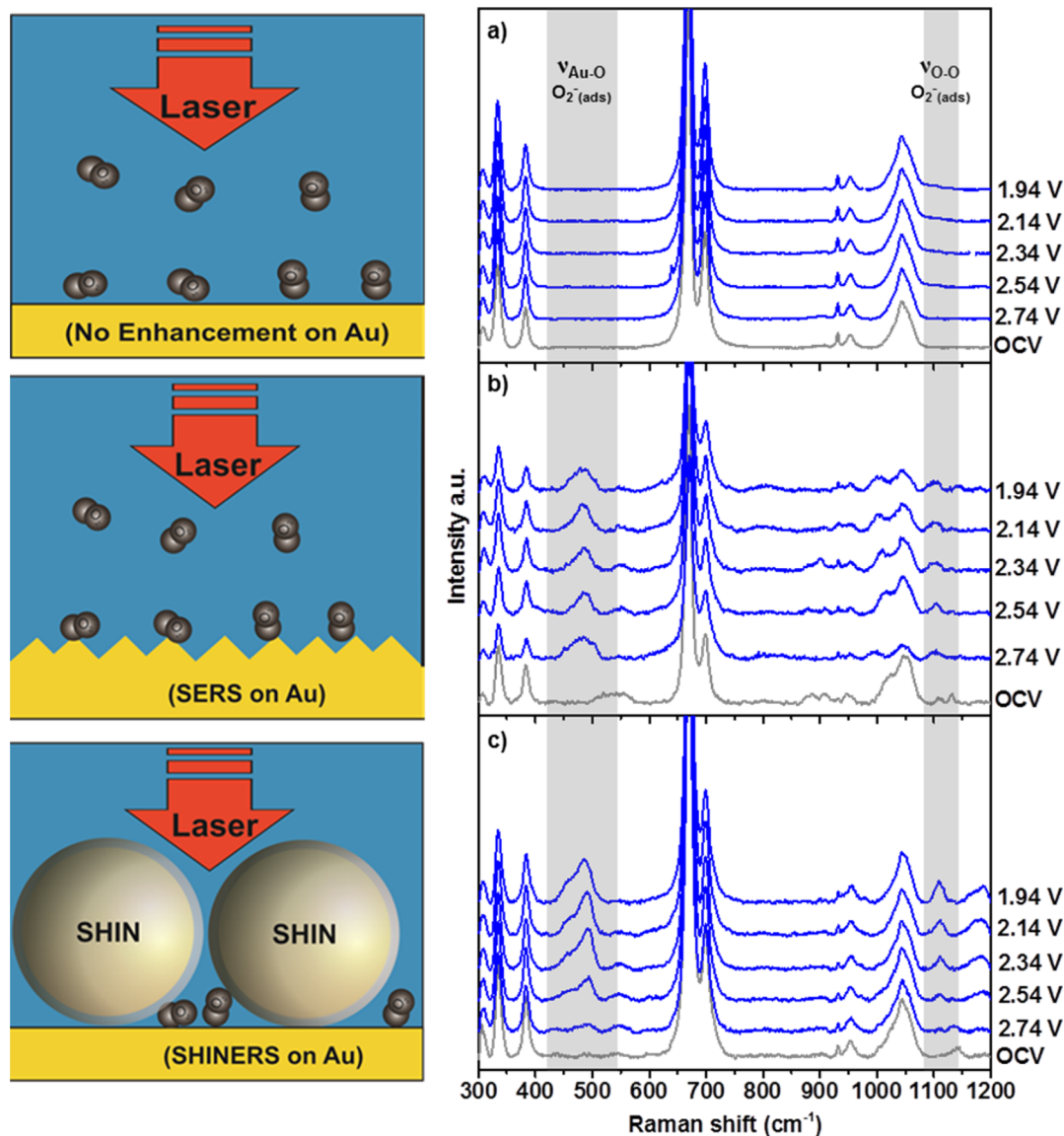


Figure 2. In situ Raman spectra of the ORR in 0.1 M TBAClO₄/DMSO electrolyte on (a) smooth, (b) roughened, and (c) SHIN's drop cast on the surface of a polycrystalline gold electrode. All potentials versus Li/Li⁺ (SHINERS particles and dioxygen are not drawn to scale).

54 than 4 nm will drastically reduce the enhancement from the Au
 55 core (Figure S1.1). The gold nanoparticle has a strong
 56 electromagnetic field that enhances the Raman signal, while
 57 the SiO₂ shell inhibits any catalytic effect from the gold core.²³
 58 The greatest enhancement from nanoparticles occurs between
 59 two SHINERS particles, where the electromagnetic field from
 60 both cores can enhance the nearby molecules, as indicated by
 61 the red areas on the scheme (Figure 1a). SHINERS can
 62 therefore enhance the Raman signal upon a variety of
 63 surfaces,^{24,25} such as carbon that has previously been very
 64 challenging to analyze. Validation of uniform silica coating and
 65 application of SHINERS are discussed in Figures S1.1–S1.5
 66 and Table S1.
 67 Studying the ORR using 0.1 M TBAClO₄ in dimethyl
 68 sulfoxide (DMSO) on a smooth polycrystalline gold electrode
 69 demonstrated that Raman spectroscopy on a surface without
 70 any enhancement is inherently weak (Figure 2a). The spectrum
 71 at open-circuit voltage (OCV) displays DMSO solvent peaks.
 72 No spectral bands were observed for the supporting salt. The
 73 lack of peaks is likely a result of no surface plasmons to enhance

the inelastically scattered photons of surface adsorbed
 74 tetrabutylammonium (TBA). Raman scans were taken at
 75 decreasing potentials down to 1.84 V. There was no change
 76 observed in peak position or intensity from the OCV spectrum
 77 at any potential.
 78

The Au surface can be electrochemically roughened prior to
 79 experiments using an oxidation–reduction cycle; this created a
 80 nanostructured surface, which leads to a distribution of charge
 81 when excited by photons,²⁶ enhancing the local electric field.
 82 The chemically adsorbed molecules can also undergo charge
 83 transfer with the surface that can, in turn, increase the
 84 polarizability.²⁷ Roughening the surface displays a notable
 85 enhancement (Figure 2b). The same electrochemical system as
 86 Figure 2a was used with a roughened gold electrode. At OCV
 87 only peaks related to DMSO were visible. The growth of two
 88 bands at 1110 ($\nu_{\text{O-O}}$) and 490 cm⁻¹ ($\nu_{\text{Au-O}}$) was observed
 89 when the potential was decreased and can be assigned to the
 90 formation of adsorbed superoxide (O₂⁻). The position of these
 91 peaks agrees well with literature.^{19,28} To confirm the origin of
 92 the observed peaks, we ran the experiment without the
 93

94 presence of oxygen, under argon. (Figure S2), and no peaks are
95 seen to grow in either the O_2^- or Au–O spectral region, within
96 similar potential cycling limits.

97 SHINs are an alternative method of enhancing the Raman
98 signal of substrate molecules on the electrode surface. In the
99 same 0.1 M TBAClO₄/DMSO electrolyte media the in situ
100 reaction on a smooth polycrystalline gold electrode was studied
101 with 2 μ L of SHINs drop cast onto the surface (Figure S3).
102 The OCV Raman spectrum only showed DMSO solvent peaks
103 in agreement with the polycrystalline surface with and without
104 surface enhancement. The in situ Raman spectra (Figure 2c)
105 between 2.84 and 1.84 V observed the growth of two peaks at
106 1110 and 490 cm^{-1} for the free O_2^- and gold oxide peaks.²⁰ A
107 comparison of the two sets of spectra for SERS and SHINERS
108 demonstrated that SHINERS is a useful technique to monitor
109 the ORR in a nonaqueous electrolyte media without loss of
110 signal intensity from the different method of phonon
111 enhancement and has been shown to provide similar data in
112 different anion salt electrolytes, such as in tetrabutylammonium
113 triflate (Figure S4). Furthermore, Figure S5 shows that SHINs
114 have no effect on the electrochemistry, as the electrochemical
115 response with and without SHINs is identical.

116 The electrochemistry of 0.1 M TBAClO₄ in DMSO saturated
117 with oxygen varies between different electrode surfaces (Figure
118 3). The reversibility of the O_2^- couple is affected when the

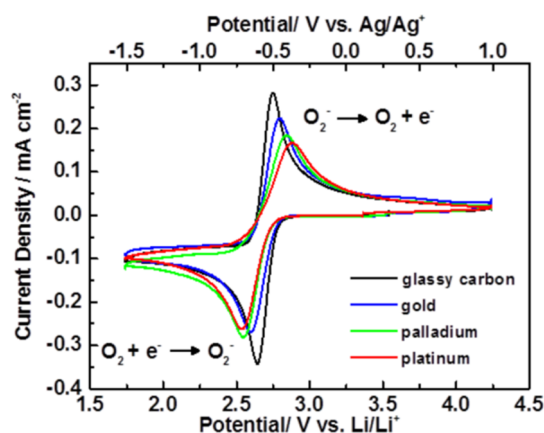


Figure 3. Cyclic voltammograms of 0.1 M TBAClO₄ in DMSO at 50 mV/s on various electrode surfaces.

119 electrode surface is changed. Glassy carbon (GC) is the most
120 reversible ($\Delta E = 90$ mV), whereas platinum is the least
121 reversible ($\Delta E = 350$ mV). The change in reversibility is
122 accounted for by the interactions of O_2^- with the surface,
123 whereby Pt has the slowest reaction kinetics of the three
124 surfaces (Pt < Pd < Au), with O_2^- being the most strongly
125 chemisorbed, which is in agreement with density function
126 theory calculations, where O_2^- is energetically favorable to
127 chemisorb to the Pt surface.²⁹ There is little interaction with
128 the surface on the GC electrode, unlike Au, Pd, and Pt, where
129 dioxygen can chemisorb.²⁹ Pt has the strongest interaction with
130 O_2^- due to the bonding of the $5d_{xx}$ and $O_2^- 2\pi^*$ orbitals in Pt,
131 giving a higher adsorption energy and shorter metal–oxygen
132 bond length than with Au. Au has a filled d orbital, so O_2^- is
133 not chemisorbed like Pt; a weaker interaction still occurs due to
134 a distortion of charge density creating an overlap of bonding
135 orbitals.²⁹ The same principle is applied for Pd (bonding of the
136 $4d_{xx}$ and $O_2^- 2\pi^*$ orbitals); however, Pd has a lower oxygen
137 binding energy than Pt.³⁰ Previous studies have shown similar

behavior on GC electrodes with different solvent electrolytes 138
such as dimethyl ether, where a change in reversibility is 139
observed due to the different solubility and kinetics, but a $1e^-$ 140
reduction mechanism is still observed.³¹ 141

The Pd surface exhibits similar behavior to the Au surface for 142
the ORR (Figure 4a). A peak at 1108 cm^{-1} for O_2^- is observed 143 144

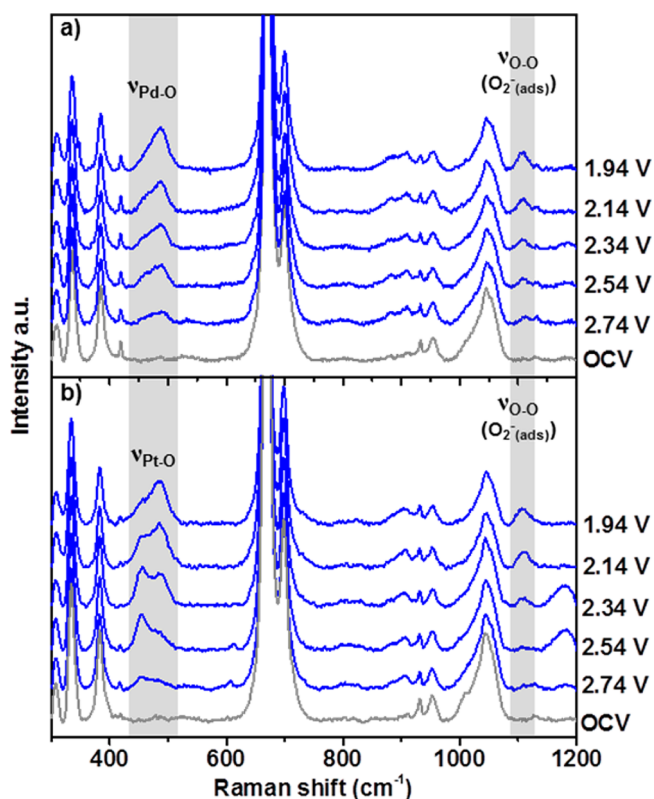


Figure 4. In situ Raman spectra of 0.1 M TBAClO₄ in DMSO saturated with O₂ on (a) Pd and (b) Pt with SHINs drop cast onto the surface. All potentials versus Li/Li⁺.

from 2.74 V and grows in intensity with negative potential, 144
correlating with cyclic voltammetry data in Figure 3. A 145
corresponding peak at 486 cm^{-1} for (ν_{Pd-O}) grows propor- 146
tionally to the O_2^- peak. The in situ Raman spectra on Pt 147
(Figure 4b) showed a variance in the spectral response in 148
comparison with Au and Pd. At 1108 cm^{-1} a peak assigned to 149
 ν_{O-O} of O_2^- grew in intensity with increasing reduction 150
potential, similar to that observed on Au and Pd; however, on 151
Pt, unlike Au and Pd, the interaction with the Pt surface was 152
different. Initially, on the Pt surface a peak was observed at the 153
lower wavenumber of 456 cm^{-1} and initially grew in intensity 154
with decreasing potential. A second peak at 484 cm^{-1} grew at 155
more negative potentials at the expense of the 456 cm^{-1} peak, 156
which then decreased in intensity. In both Figures 2c and 4b, 157
a small band at 1179 cm^{-1} is observed to appear (and diminish 158
in the case of Pt); its assignment will be discussed later within this 159
paper. 160

The SHINERS data demonstrate variation of O_2^- interaction 161
between Pt and the other two metal surfaces (Figure S6 and 162
Table S2). All three surfaces exhibit a shoulder at 456 cm^{-1} ; for 163
Au and Pd this remains a shoulder on the peak around 490 164
 cm^{-1} . Pt favors the peak at 456 cm^{-1} at lower reduction 165
potentials; as the potential decreases the peak at 490 cm^{-1} 166
becomes dominant. It is likely the two peaks originate from 167

168 different vibrational stretching modes of O_2^- adsorbed on the
169 metal surface.³² At lower potentials, there is a lower surface
170 coverage of O_2^- on the Pt, allowing the O_2^- to have a flat
171 orientation; with increasing negative reduction potentials, an
172 end on orientation is favored. This could account for the flat
173 conformation rather than the end on conformation on Pt,
174 unlike Au and Pd, which favor the end on conformation due to
175 a weaker interaction with the surface of the electrode.²⁹
176 Furthermore, the interaction of the solvent with the electrode
177 surface also needs to be taken into account; at less negative
178 potentials DMSO may passivate the surface, preventing the
179 onset of dioxygen adsorption. Future studies using single-crystal
180 electrodes with SHINERS would be required to clarify the exact
181 mechanism taking place at the platinum surface, in combination
182 with appropriate level theory calculations.

183 The GC surface exhibits different behavior to the metal
184 surfaces previously analyzed (Figure 5). There was no Raman

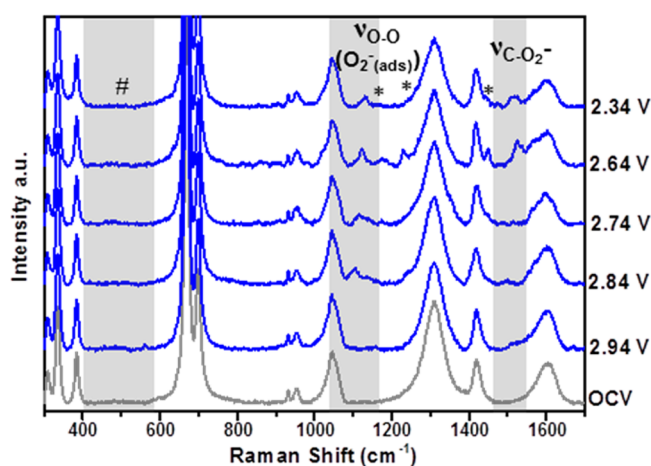


Figure 5. In situ Raman spectra of 0.1 M TBAClO₄/DMSO with O₂ on a GC electrode with SHINs drop cast onto the electrode surface. Potentials versus Li/Li⁺.

185 peak observed between 400 and 550 cm⁻¹ at any potential on the
186 GC electrode surface. Thereby, there is an absence of a
187 metal–O₂⁻ interaction (area indicated via a #), and this
188 indicates that the SHINERS particles are pinhole-free (Figures
189 S1.1–S1.4). This provides strong verification that the O₂⁻ peak
190 (ν_{O-O}) at ~1110 cm⁻¹ originates solely from its interaction at
191 the GC surface, not with the gold core of the SHIN, with it
192 being detected solely due to the Raman enhancement from the
193 SHIN particles. The formation of O₂⁻ on the GC surface
194 occurred below 2.84 V in the reduction sweep at 1107 cm⁻¹,
195 and the band shifts positively to 1123 cm⁻¹ with decreasing
196 potential.³³ At lower potential, O₂⁻ is bound at more favorable
197 sites on the surface, and with increasing concentration O₂⁻ is
198 forced into less favorable sites, reducing the interaction with the
199 surface, causing a positive shift in the Raman band; this
200 coincides with a peak at 1520 cm⁻¹ that could be a result of the
201 interaction of O₂⁻ with the graphitic rings in the carbon.³⁴ The
202 interaction of the O₂⁻ with the graphitic ring could increase
203 with decreasing potential, creating greater distortion with the
204 ring and accounting for the wavenumber shift of the O₂⁻ peak.
205 Figure S7 confirms that the 1520 cm⁻¹ band is unique to
206 carbon substrate because it is not observed on Au within an
207 extended wavenumber range.

208 SHINERS on GC also displayed bands at 1179 (as seen in
209 Figures 2c and 4b), 1230, and 1450 cm⁻¹ that coincide with

ORR (Figure 5). No potential-dependent electrolyte bands 210
could be assigned to these peaks nor known reduced oxygen 211
salts (Figures S8 and S9).²⁰ We speculate that 1179 cm⁻¹ could 212
be assigned to HO₂, as its position is close to the band at 1165 213
cm⁻¹ identified by the group of Gewirth of HO₂ adsorbed onto 214
Au in perchloric acid (HClO₄) solution.³⁵ Concurrently, the 215
band at 1450 cm⁻¹ can be then tentatively assigned as ν_{HO_2-C} 216
C, with the band at 1230 cm⁻¹ remaining as yet unassigned. 217
Strict drying protocol ensured that all measurements took place 218
in H₂O content below 20 ppm, as determined by Karl Fisher 219
titration. Thereby we believe the nature of the measurements is 220
sensitive to trace water contamination. Certainly further 221
investigations using SHINERS to understand the effect of 222
water concentration on these bands with the use of isotopic 223
labeling to strengthen band assignments is warranted. 224

SHINERS was then employed to investigate ORR in the 225
presence of Li⁺ in low (acetonitrile–MeCN) and high 226
(DMSO) donor number solvents, with corresponding electro- 227
chemistry in Figure S10. In 0.5 M LiClO₄, MeCN (Figure 6a), 228 66

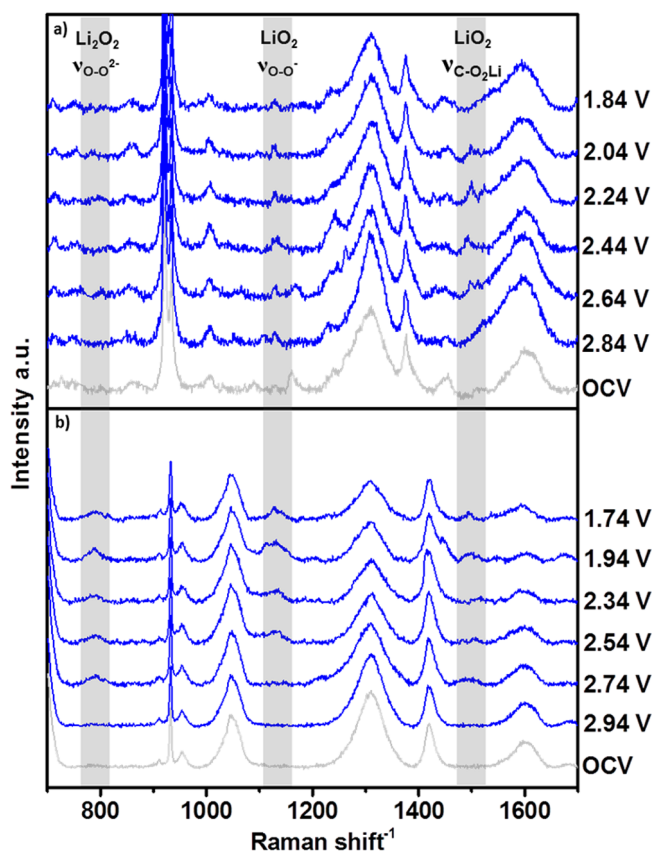
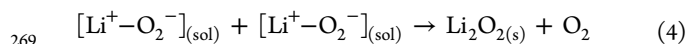
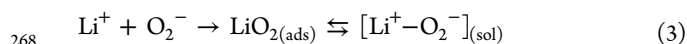
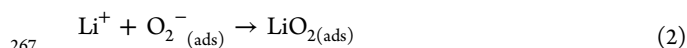


Figure 6. In situ Raman spectra on a GC electrode with SHINs in 0.5 M LiClO₄ in (a) MeCN and (b) DMSO. All potentials versus Li/Li⁺.

SHINERS detected the growth of LiO₂ at 1125 cm⁻¹ on GC 229
below 2.84 V, with Li₂O₂ not detected, due to the absence of 230
the main peroxide band at 790 cm⁻¹. In addition, a peak at 231
1500 cm⁻¹ was observed in the MeCN Raman spectra at lower 232
reduction potentials. This peak is likely the result of LiO₂ 233
interacting with a vibrational mode of the graphitic ring³⁴ 234
(Table S3). SHINERS on GC in 0.5 M LiClO₄, DMSO (Figure 235
6b), showed the appearance of Li₂O₂ at 790 cm⁻¹ at 2.74 V, 236
which remained as the potential decreased further to 1.74 V. At 237
2.74 V, bands pertaining to LiO₂ at 1128 cm⁻¹ and LiO₂–C at 238

239 1500 cm⁻¹ were also detected on the GC electrode. The
 240 appearance of LiO₂ is indicative of a mechanism, where both
 241 Li₂O₂ and LiO₂ are formed as stable products on the GC
 242 surface. The proposed decomposition reaction of DMSO to
 243 dimethyl sulfone (DMSO₂) was unable to be established in our
 244 measurements due to the absence of a peak around 1142
 245 cm⁻¹.³⁶

246 The data reported herein on GC are suggestive of a reaction
 247 mechanism that is both surface- and solvent-dependent. The
 248 solvation of the Li⁺ cation in MeCN is lower due to a positive
 249 Gibbs free energy; therefore, ORR occurs on the surface and
 250 LiO₂ will be observed on the electrode¹⁹ (eqs 1 and 2). The
 251 interaction of LiO₂ with the carbon surface appears to stabilize
 252 the adsorbed LiO₂ species, and within the experiment, no Li₂O₂
 253 formation is observed to occur from a second electron transfer
 254 or via disproportionation. This observation agrees with work of
 255 Lu et al.³⁷ that shows the stable cycling of LiO₂. In DMSO (eqs
 256 1, 3, and 4), a partial surface/solution mechanism occurs,
 257 whereby both Li₂O₂ and LiO₂ are formed as the major
 258 reduction products, which is contrary to what has been
 259 reported on Au electrode substrates.¹⁹ LiO₂ is also bound to the
 260 carbon surface in DMSO (1500 cm⁻¹). LiO₂ can then desorb
 261 and diffuse into the bulk electrolyte, where it can disproportion-
 262 ate to give Li₂O₂ in agreement with data published by Ye et
 263 al.³⁸ Li₂CO₃ was not detected during ORR on GC, implying
 264 that the decomposition of the carbon electrode was negligible
 265 during the time frame of the measurement (Figure S9).



270 SHINERS has been demonstrated as an effective method of
 271 detecting intermediate species and ORR products on an array
 272 of electrode substrates, such as Pt, Pd and GC, which
 273 previously SERS has been unable to access. The consistency
 274 of SHINERS has been validated by its ability to reproduce data
 275 gathered using SERS in the same electrolyte media on Au
 276 electrode surfaces. Notably the metal-superoxide band shape
 277 varies between the noble metals depending on superoxide
 278 interaction at the surface. The use of SHINERS in the presence
 279 of Li⁺ has shown that both surface and solvent can be harnessed
 280 to influence ORR pathways, which may be critical in designing
 281 electrode/electrolyte interfaces that can minimize side reactions
 282 within Li–O₂ cells. This work provides a strong platform to
 283 study more complex electrolyte and electrode systems with
 284 SHINERS particles.

285 ■ ASSOCIATED CONTENT

286 ● Supporting Information

287 The Supporting Information is available free of charge on the
 288 ACS Publications website at DOI: 10.1021/acs.jpcllett.6b00730.

289 Methods section, SHIN preparation, synthesis and
 290 validation, transfer onto electrode surfaces and enhance-
 291 ment factor of SHIN particles, supporting electro-
 292 chemical data, Raman spectra of materials used, Raman
 293 peak analysis comparison of superoxide on metal
 294 surfaces, and SERS and SHINERS experiments under
 295 argon deoxygenated electrolytes. (PDF)

■ AUTHOR INFORMATION

Corresponding Author

*E-mail: hardwick@liverpool.ac.uk.

Notes

The authors declare no competing financial interest.

■ ACKNOWLEDGMENTS

Professor Jian-Feng Li and Jin Chao Dong (Xiamen University) are acknowledged for their knowledge and assistance and access to their facilities in learning the synthesis and procedure for SHINERS. Professor Richard Nichols and the Electronanomat Exchange Program are acknowledged. Dr. Sarah Ball, Dr. Mark Copley, Johnson Matthey, and the Engineering and Physical Sciences Research Council (EPSRC) CASE award are acknowledged. Dr. Tobias Heil and the Nanoinvestigation Centre at Liverpool (NiCaL) are acknowledged for access to their TEM. Support from the EPSRC grant EP/J020265/1 is also gratefully acknowledged.

■ REFERENCES

- (1) Cheng, F.; Chen, J. Metal-Air Batteries: From Oxygen Reduction Electrochemistry to Cathode Catalysts. *Chem. Soc. Rev.* **2012**, *41*, 2172–2192.
- (2) Rahman, M. A.; Wang, X.; Wen, C. High Energy Density Metal-Air Batteries: A Review. *J. Electrochem. Soc.* **2013**, *160*, A1759–A1771.
- (3) Bruce, P. G.; Freunberger, S. A.; Hardwick, L. J.; Tarascon, J. M. Li–O₂ and Li–S Batteries with High Energy Storage. *Nat. Mater.* **2011**, *11*, 19–29.
- (4) Tarascon, J. M. Key Challenges in Future Li–Battery Research. *Philos. Trans. R. Soc., A* **2010**, *368*, 3227–3241.
- (5) Girishkumar, G.; McCloskey, B.; Luntz, A. C.; Swanson, S.; Wilcke, W. Lithium–Air Battery: Promise and Challenges. *J. Phys. Chem. Lett.* **2010**, *1*, 2193–2203.
- (6) Zhang, J. *PEM Fuel Cell Electrocatalysts and Catalyst Layers: Fundamentals and Applications*; Springer: London, 2008.
- (7) Sawyer, D. *Oxygen Chemistry*; Oxford University Press, 1991.
- (8) Lodge, A. W.; Lacey, M. J.; Fitt, M.; Garcia-Araez, N.; Owen, J. R. Critical Appraisal on the Role of Catalysts for the Oxygen Reduction Reaction in Lithium–Oxygen Batteries. *Electrochim. Acta* **2014**, *140*, 168–173.
- (9) Padmanabhan, V. J.; Berry, N. G.; Papageorgiou, G.; Nichols, R. J.; Hardwick, L. J. Mechanistic Insight into the Superoxide Induced Ring Opening in Propylene Carbonate Based Electrolytes using in situ Surface-Enhanced Infrared Spectroscopy. *J. Am. Chem. Soc.* **2016**, *138*, 3745–3751.
- (10) Peng, Z. Q.; Freunberger, S. A.; Hardwick, L. J.; Chen, Y. H.; Giordani, V.; Barde, F.; Novak, P.; Graham, D.; Tarascon, J. M.; Bruce, P. G. Oxygen Reactions in a Non-Aqueous Li⁺ Electrolyte. *Angew. Chem., Int. Ed.* **2011**, *50*, 6351–6355.
- (11) Sharon, D.; Etacheri, V.; Garsuch, A.; Afri, M.; Frimer, A. A.; Aurbach, D. On the Challenge of Electrolyte Solutions for Li–Air Batteries: Monitoring Oxygen Reduction and Related Reactions in Polyether Solutions by Spectroscopy and EQCM. *J. Phys. Chem. Lett.* **2013**, *4*, 127–131.
- (12) Trahan, M. J.; Mukerjee, S.; Plichta, E. J.; Hendrickson, M. A.; Abraham, K. M. Studies of Li–Air Cells Utilizing Dimethyl Sulfoxide-Based Electrolyte. *J. Electrochem. Soc.* **2013**, *160*, A259–A267.
- (13) Mozshukhina, N.; Méndez De Leo, L. P.; Calvo, E. J. Infrared Spectroscopy Studies on Stability of Dimethyl Sulfoxide for Application in a Li–Air Battery. *J. Phys. Chem. C* **2013**, *117*, 18375–18380.
- (14) Tian, Z. Q. Surface-enhanced Raman spectroscopy: advancements and applications. *J. Raman Spectrosc.* **2005**, *36*, 466–470.
- (15) Gittleson, F. S.; Yao, K. P. C.; Kwabi, D. G.; Sayed, S. Y.; Ryu, W. H.; Shao-Horn, Y.; Taylor, A. D. Raman Spectroscopy in Lithium–Oxygen Battery Systems. *ChemElectroChem* **2015**, *2*, 1446–1457.

- 360 (16) Otto, A.; Mrozek, I.; Grabhorn, H.; Akemann, W. Surface
361 Enhanced Raman Scattering. *J. Phys.: Condens. Matter* **1992**, *4*, 1143–
362 1212.
- 363 (17) Wu, D.-Y.; Li, J.-F.; Ren, B.; Tian, Z. Q. Electrochemical
364 Surface-Enhanced Raman Spectroscopy of Nanostructures. *Chem. Soc.*
365 *Rev.* **2008**, *37*, 1025–1041.
- 366 (18) Laoire, C. O.; Mukerjee, S.; Abraham, K. M.; Plichta, E. J.;
367 Hendrickson, M. A. Elucidating the Mechanism of Oxygen Reduction
368 for Lithium-Air Battery Applications. *J. Phys. Chem. C* **2009**, *113*,
369 20127–20134.
- 370 (19) Johnson, L.; Li, C. M.; Liu, Z.; Chen, Y. H.; Freunberger, S. A.;
371 Ashok, P. C.; Praveen, B. B.; Dholakia, K.; Tarascon, J. M.; Bruce, P.
372 G. The role of LiO₂ Solubility in O₂ Reduction in Aprotic Solvents and
373 its Consequences for LiO₂ Batteries. *Nat. Chem.* **2014**, *6*, 1091–1099.
- 374 (20) Aldous, I. M.; Hardwick, L. J. Influence of Tetraalkylammonium
375 Cation Chain Length on Gold and Glassy Carbon Electrode Interfaces
376 for Alkali Metal-Oxygen Batteries. *J. Phys. Chem. Lett.* **2014**, *5*, 3924–
377 3930.
- 378 (21) Hardwick, L. J.; Bruce, P. G. The Pursuit of Rechargeable Non-
379 Aqueous Lithium-Oxygen Battery Cathodes. *Curr. Opin. Solid State*
380 *Mater. Sci.* **2012**, *16*, 178–185.
- 381 (22) Li, J. F.; Huang, Y. F.; Ding, Y.; Yang, Z. L.; Li, S. B.; Zhou, X.
382 S.; Fan, F. R.; Zhang, W.; Zhou, Z. Y.; Wu, D. Y.; Ren, B.; Wang, Z. L.;
383 Tian, Z. Q. Shell-Isolated Nanoparticle-Enhanced Raman Spectroscopy.
384 *Nature* **2010**, *464*, 392–395.
- 385 (23) Li, J. F.; Tian, X. D.; Li, S. B.; Anema, J. R.; Yang, Z. L.; Ding, Y.;
386 Wu, Y. F.; Zeng, Y. M.; Chen, Q. Z.; Ren, B.; Wang, Z. L.; Tian, Z. Q.
387 Surface Analysis using Shell-Isolated Nanoparticle-Enhanced Raman
388 Spectroscopy. *Nat. Protoc.* **2012**, *8*, 52–65.
- 389 (24) Huang, Y.-F.; Li, C.-Y.; Broadwell, L.; Li, J. F.; Wu, D. Y.; Ren,
390 B.; Tian, Z. Q. Shell-Isolated Nanoparticle-Enhanced Raman Spec-
391 troscopy of Pyridine on Smooth Silver Electrodes. *Electrochim. Acta*
392 **2011**, *56*, 10652–10657.
- 393 (25) Li, J. F.; Ding, S. Y.; Yang, Z. L.; Bai, M. L.; Anema, J. R.; Wang,
394 X.; Wang, A.; Wu, D. Y.; Ren, B.; Hou, S. M.; Wandlowski, T.; Tian, Z.
395 Q. Extraordinary Enhancement of Raman Scattering from Pyridine on
396 Single Crystal Au and Pt Electrodes by Shell-Isolated Au Nano-
397 particles. *J. Am. Chem. Soc.* **2011**, *133*, 15922–15925.
- 398 (26) Kneipp, K.; Moskovits, M.; Kneipp, H. *Surface-Enhanced Raman*
399 *Scattering: Physics and Applications*; Physica-Verlag, 2006.
- 400 (27) Aroca, R. *Surface-Enhanced Vibrational Spectroscopy*; Wiley,
401 2006.
- 402 (28) Socrates, G. *Infrared and Raman Characteristic Group*
403 *Frequencies: Tables and Charts*; Wiley, 2001.
- 404 (29) Zhuang, G. V.; Markovic, N. M.; Ross, P. N.; Meeting, E. S.
405 Power Source Modeling: Proceedings of the International Symposium.
406 *Proc. - Electrochem. Society* **2002**, *30*, 63–73.
- 407 (30) Norskov, J.K.; Rossmeisl, J.; Logadottir, A.; Lindqvist, L.;
408 Kitchin, J. R.; Bligaard, T.; Jonsson, H. Origin of the Overpotential for
409 the Oxygen Reduction at a Fuel-Cell Cathode. *J. Phys. Chem. B* **2004**,
410 *108*, 17886–17892.
- 411 (31) Laoire, C. O.; Mukerjee, S.; Abraham, K. M.; Plichta, E. J.;
412 Hendrickson, M. A. Influence of Non-Aqueous Solvents on the
413 Electrochemistry of Oxygen in the Rechargeable Lithium-Air Battery.
414 *J. Phys. Chem. C* **2010**, *114*, 9178–9186.
- 415 (32) McBride, J. R.; Graham, G. W.; Peters, C. R.; Weber, W. H.
416 Growth and Characterization of Reactively Sputtered Thin-Film
417 Platinum Oxides. *J. Appl. Phys.* **1991**, *69*, 1596–1604.
- 418 (33) Yang, H. H.; McCreery, R. L. Elucidation of the Mechanism of
419 Dioxygen Reduction on Metal-Free Carbon Electrodes. *J. Electrochem.*
420 *Soc.* **2000**, *147*, 3420–3428.
- 421 (34) Zhai, D.; Wang, H. H.; Lau, K. C.; Gao, J.; Redfern, P. C.; Kang,
422 F.; Li, B.; Indacochea, E.; Das, U.; Sun, H.; Sun, H. H.; Amine, K.;
423 Curtiss, L. A. Raman Evidence for Late Stage Disproportionation in a
424 Li-O₂ Battery. *J. Phys. Chem. Lett.* **2014**, *5*, 2705–2710.
- 425 (35) Li, X.; Gewirth, A. Oxygen Electroreduction through a
426 Superoxide Intermediate on Bi-Modified Au Surfaces. *J. Am. Chem.*
427 *Soc.* **2005**, *127*, 5252–5260.
- (36) Schroeder, M. A.; Kumar, N.; Pearse, A. J.; Liu, C.; Lee, S. B.; 428
Rubloff, G. W.; Leung, K.; Noked, M. DMSO-Li₂O₂ Interface in the 429
Rechargeable Li-O₂ Battery Cathode: Theoretical and Experimental 430
Perspectives on Stability. *ACS Appl. Mater. Interfaces* **2015**, *7*, 11402– 431
11411. 432
- (37) Lu, J.; Lee, Y. J.; Luo, X.; Lau, K. C.; Asadi, M.; Wang, H. H.; 433
Brombosz, S.; Wen, J.; Zhai, D.; Chen, Z.; et al. A Lithium-Oxygen 434
Battery based on Lithium Superoxide. *Nature* **2016**, *529*, 377–382. 435
- (38) Qiao, Y.; Ye, S. Spectroscopic Investigation for Oxygen 436
Reduction and Evolution Reactions on Carbon Electrodes in Li-O₂ 437
Battery. *J. Phys. Chem. C* **2016**, *120*, 8033–8047. 438